Electronic Supplementary Material (ESI) for Journal of Materials Chemistry A.
This journal is © The Royal Society of Chemistry 2015

Supplementary information

Use of a protic salt for the formation of liquid-crystalline proton-conductive complexes with mesomorphic diols

Akihiro Yamashita[a], Masafumi Yoshio,*[a] Bartolome Soberats,[ab] Hiroyuki Ohno[c] and Takashi Kato*[ab]

[a]Department of Chemistry and Biotechnology, School of Engineering, The University of Tokyo, Hongo, Bunkyo-ku, Tokyo 113-8656, Japan.
[b]CREST, JST, 4-1-8, Honcho, Kawaguchi, Saitama 332-0012, Japan.
[c]Department of Biotechnology, Tokyo University of Agriculture and Technology, Nakacho, Koganei, Tokyo 184-8588, Japan.

*Corresponding author. E-mail: kato@chiral.t.u-tokyo.ac.jp, yoshio@chembio.t.u-tokyo.ac.jp

Table of contents:

1. ^{1}H NMR spectra of protic salt 3

Protic salt **3** was identified by ^{1}H NMR spectroscopy of the $CDCl_3$ (Fig. S3) and DMSO-d_6 solution (Fig. S4). The imidazole NH proton and sulfonic acid proton are not observed for the $CDCl_3$ solution (Fig. S3). In contrast, the DMSO-d_6 solution indicates a broad signal at 14.3 ppm, which is attributable to the imidazolium NH proton.

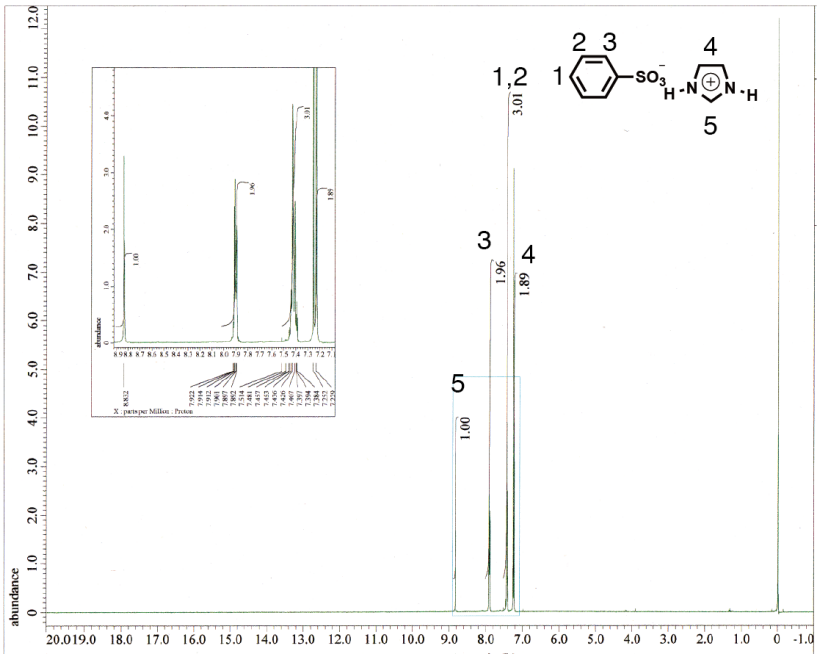

Figure S1. ^{1}H NMR spectrum of protic salt **3** in $CDCl_3$.

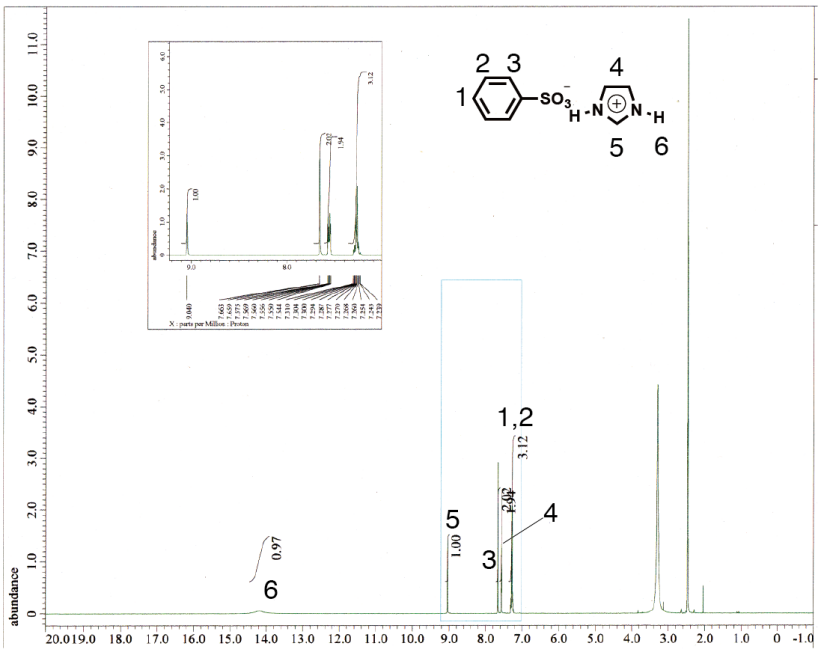

Figure S2. ^{1}H NMR spectrum of protic salt **3** in DMSO-d_6.

2. XRD diffraction study of compound 1

The self-assembled structure of compound **1** was determined by XRD measurements. The wide- angle XRD pattern of **1** at 70 °C shows four peaks corresponding to the diffraction from the (100), (110), (200) and (300) planes of the hexagonal columnar structure. The two-dimensional transmission image of small-angle XRD pattern of **1** aligned homeotropically on a polyimide film at 70 °C shows diffraction spots with a six fold symmetry from the (100) plane.

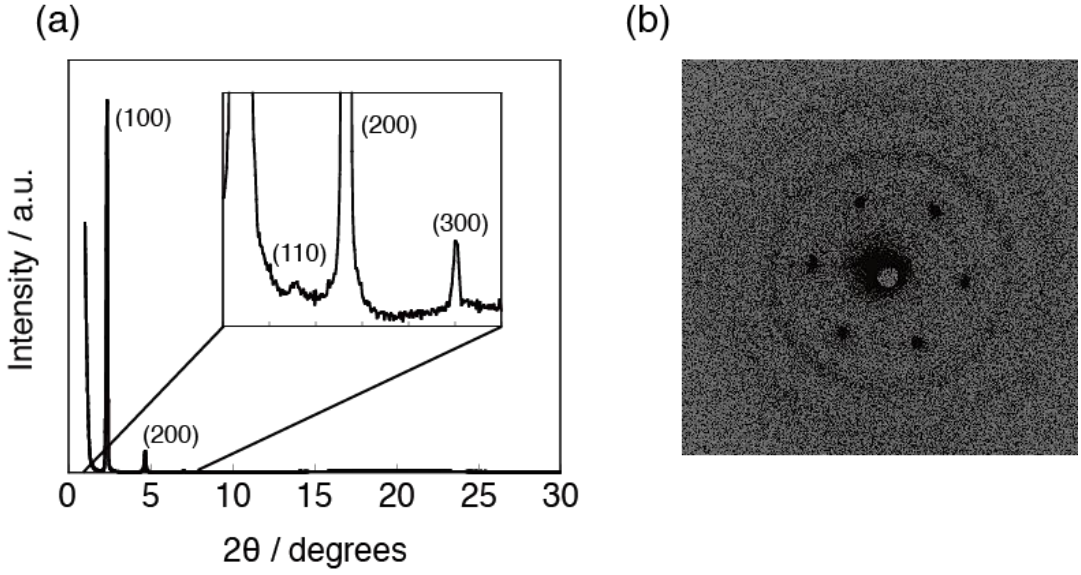

Figure S3. (a) Wide-angle and (b) small-angle XRD patterns of compound **1** in the columnar phase at 70 °C.

3. The intercolumnar distance (*a*) and average number of molecules per cross-sectional slice of the columns (*n*)

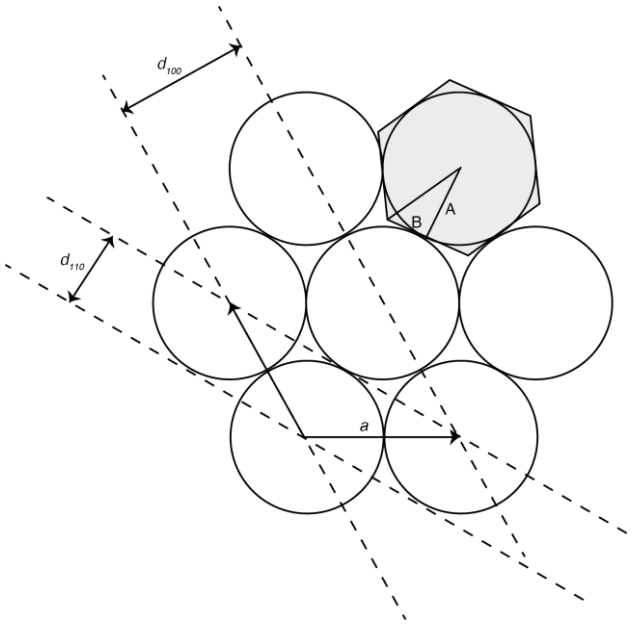

Figure S4. Schematic illustration of the hexagonal columnar lattice.

The intercolumnar distance (a) of the single diol compound and the mixtures containing protic salt **3** is estimated as follows. The value of d_{100} is obtained from the wide-angle XRD patterns.

$$a = \frac{2 \times d_{100}}{\sqrt{3}}$$

The volume of the cross-sectional slice of the column (V) is described as follows,

$$V = A \times B \times \frac{1}{2} \times 12 \times h = \frac{\sqrt{3}}{2} a^2 h$$

where h is the average spacing between benzene rings or molten alkyl chains in the direction of the column axis. The h value is estimated to be 4.5-4.6 Å from the halo around 20 ° in the wide-angle XRD patterns.

The density (ρ) of the material is described as follows:

$$\rho = \frac{\frac{n_1}{N_A} M_1 + \frac{n_3}{N_A} M_3}{V} = \frac{\frac{n_1}{N_A} M_1 + \frac{n_3}{N_A} M_3}{\frac{\sqrt{3}}{2} a^2 h} = \frac{2}{\sqrt{3}} \frac{n_1 M_1 + n_3 M_3}{N_A a^2 h}$$

where n_1 and n_3 are the average number of molecules of compound **1** and protic salt **3** per cross-sectional slice of the columns respectively, M_1 and M_3 are the molecular weight of **1** and **3** (M_1 = 564.9 and M_3 = 226.3). N_A is Avogadro's number (6.02×10^{23} mol^{-1}).

Therefore, n_1 and n_3 can be obtained by solving the following simultaneous equations.

$$\begin{cases} n_1 : n_3 = (100 - \mathrm{x}) : \mathrm{x} \\ n_1 M_1 + n_3 M_3 = \frac{\sqrt{3}}{2} N_A a^2 h \rho \end{cases}$$

where x is the mole% of **3** in the mixtures. The density of the diol compounds and the mixtures containing **3** is assumed to be 1.0 g cm^{-3}.

The intercolumnar distance (a) of the mixtures **1**/**3**(x) and **2**/**3**(x) up to x = 40 are shown in Figure S5. The average number of diol molecules **1** (n_1) and **2** (n_2) and protic salt (n_3) in the mixtures per cross-sectional slice of the columns are shown in Figure S6 and S7.

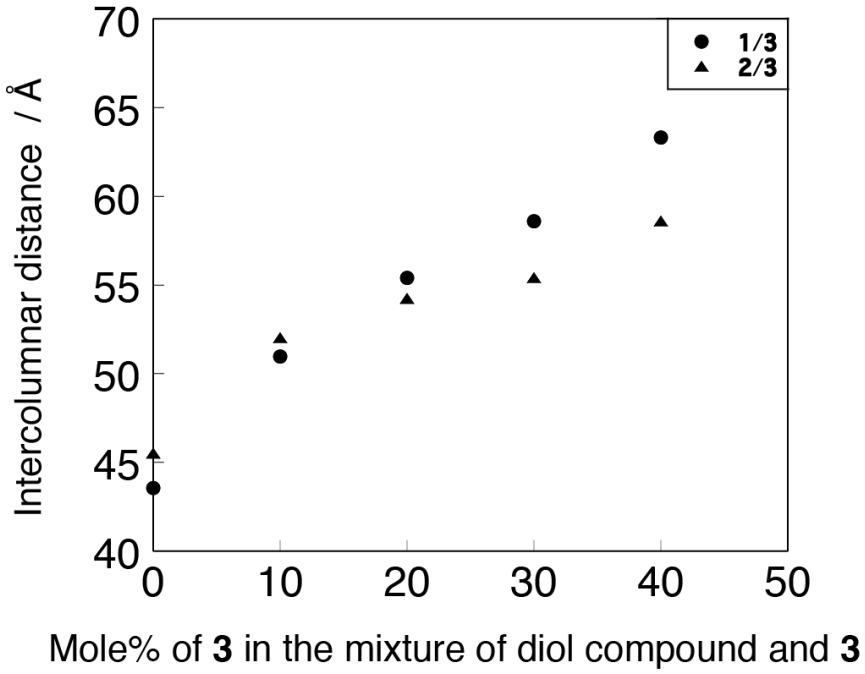

Figure S5. Intercolumnar distance of the mixtures in the Col_h phase.

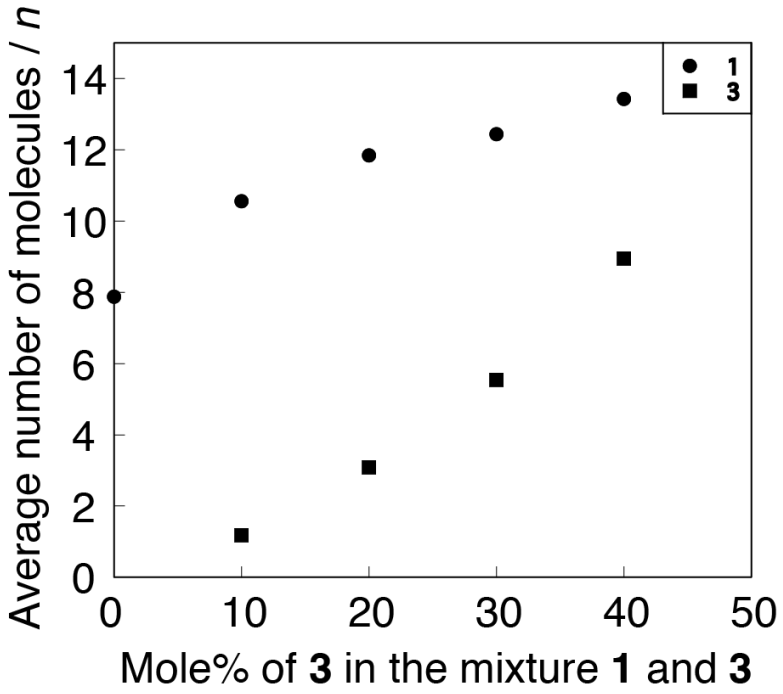

Figure S6. Average number of diol compound **1** (n_1: ●) and protic salt **3** (n_3: ■) per cross-sectional slice of the columns.

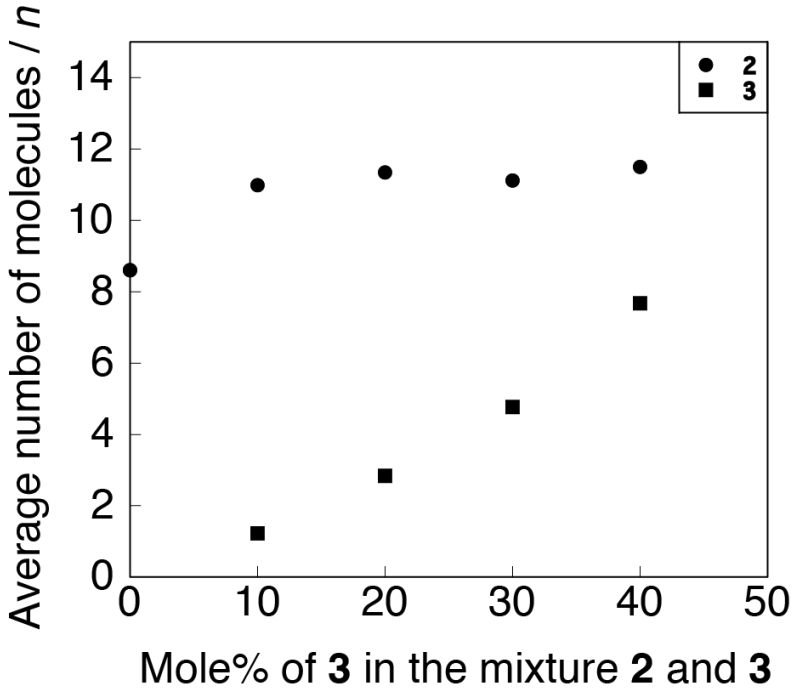

Figure S7. Average number of diol compound **2** (n_2: ●) and protic salt **3** (n_3: ■) per cross-sectional slice of the columns.

4. ^{1}H NMR spectra of 1,3, and the mixture 1/3(50)

The interactions of diol compound **1** and protic salt **3** were examined by ^{1}H NMR. The downfield shift of C(2) proton (H13) of imidazolium cation of **3** was observed.

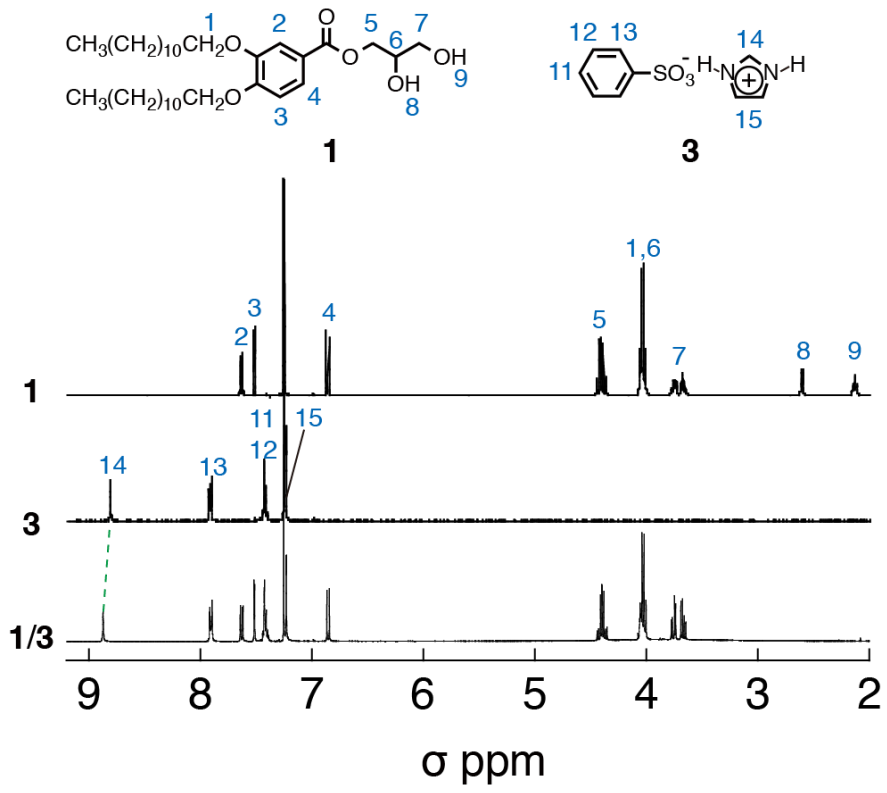

Figure S8. ^{1}H NMR spectra of diol **1**, protic salt **3**, and the equimolar mixture of **1** and **3**.

5. ^{13}C NMR spectra of 1, 2, 3, 1/3(50), and 2/3(50)

The interactions of diol compound and protic salt were examined by ^{13}C NMR. The carbonyl carbons of **1** and **2** appear at 167.2 ppm 169.2 ppm, respectively. No shifts of the carbonyl carbon are observed for the mixture s **1**/**3**(50) and **2**/**3**(50). These results suggest the carbonyl groups are not involved in specific interactions with protic salt **3**.

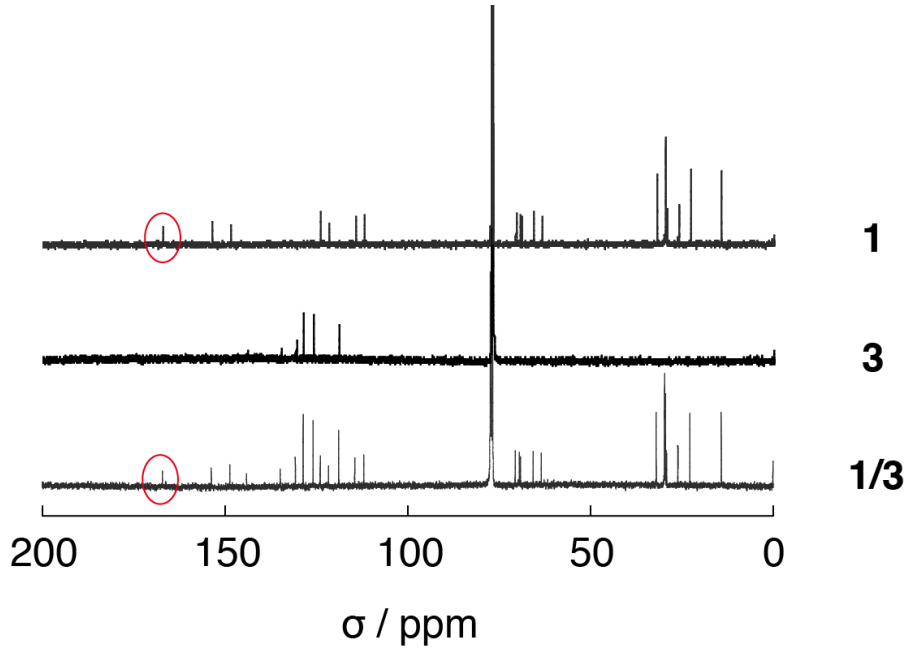

Figure S9. ^{13}C NMR spectra of single compound **1** and **3** and equimolar mixture **1/3**.

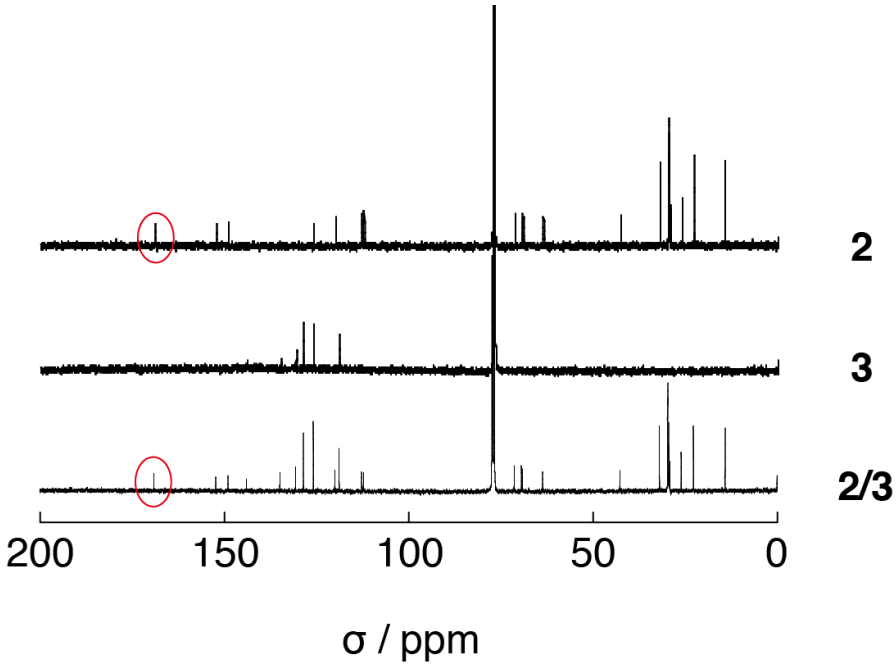

Figure S10. ^{13}C NMR spectra of single compound **2** and **3** and equimolar mixture **2/3**.

6. IR spectra of single compounds 1-3 and the mixtures

The interactions of diol compounds **1**, **2** and protic salt **3** were examined by FT-IR measurements. The IR spectra of single compounds **1**, **2**, and **3** are shown in Figure S11-S13, respectively. Figures S14-S17 indicate the IR spectra of the mixtures of **1**, **2** with **3**. The IR spectra of the mixtures containing **3** at the different concentration were also recorded (Fig. S18).

vi

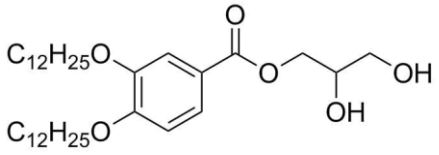

1

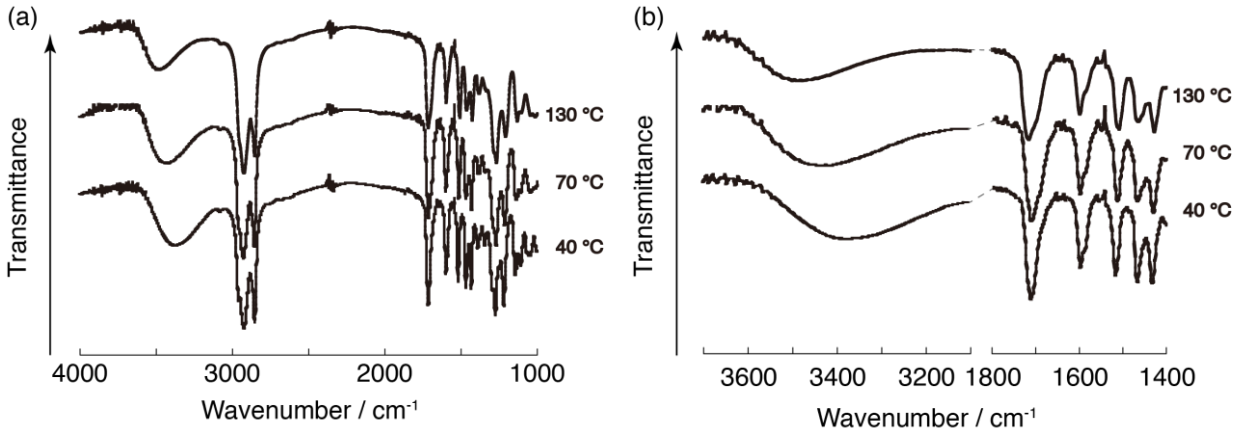

Figure S11. (a) Temperature dependent FT-IR spectra of compound **1** and (b) its enlarged view.

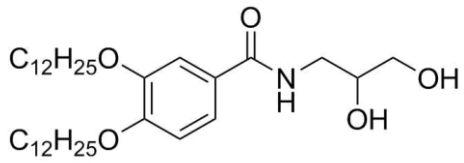

2

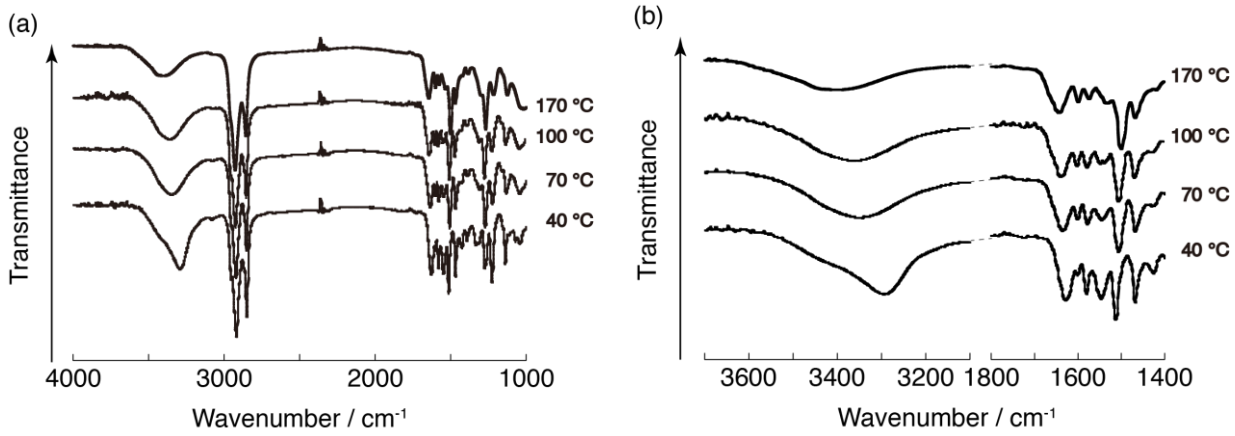

Figure S12. (a) Temperature dependent FT-IR spectra of compound **2** and (b) its enlarged view.

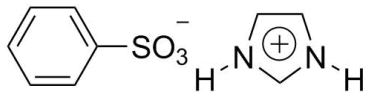

3

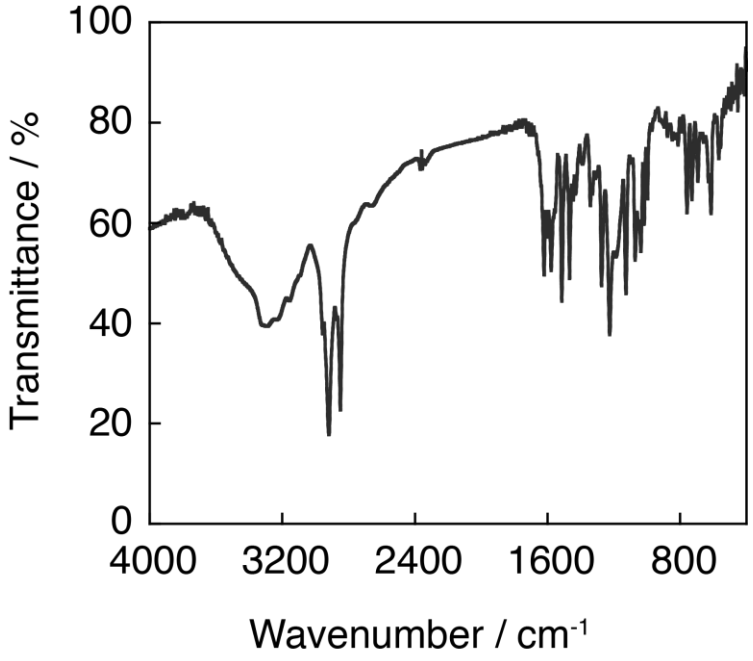

Figure S13. FT-IR spectra of protic salt **3** at room temperature.

For single compounds **1** and **2**, the O-H stretching band around 3400 cm^{-1} is shifted to higher wavenumber as the temperature rises. The N-H and C=O bands are also slightly shifted to higher wavenumber.

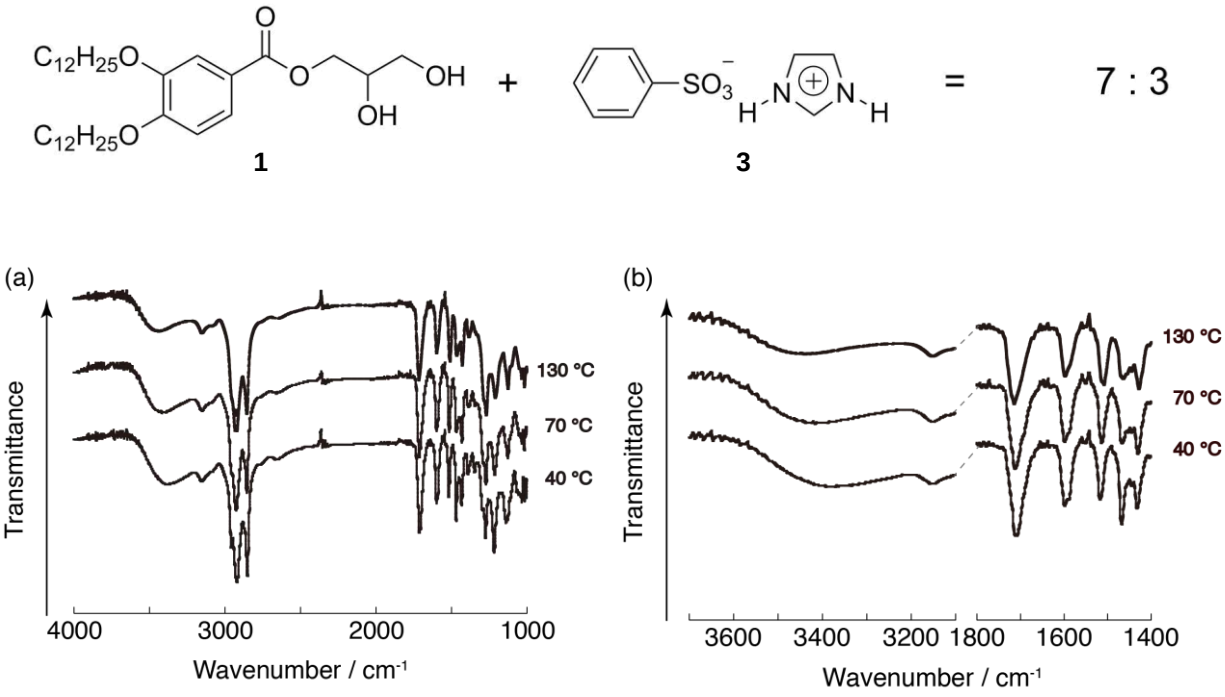

Figure S14. (a) Temperature dependent FT-IR spectra of the mixture **1**/**3**(30) and (b) its enlarged view.

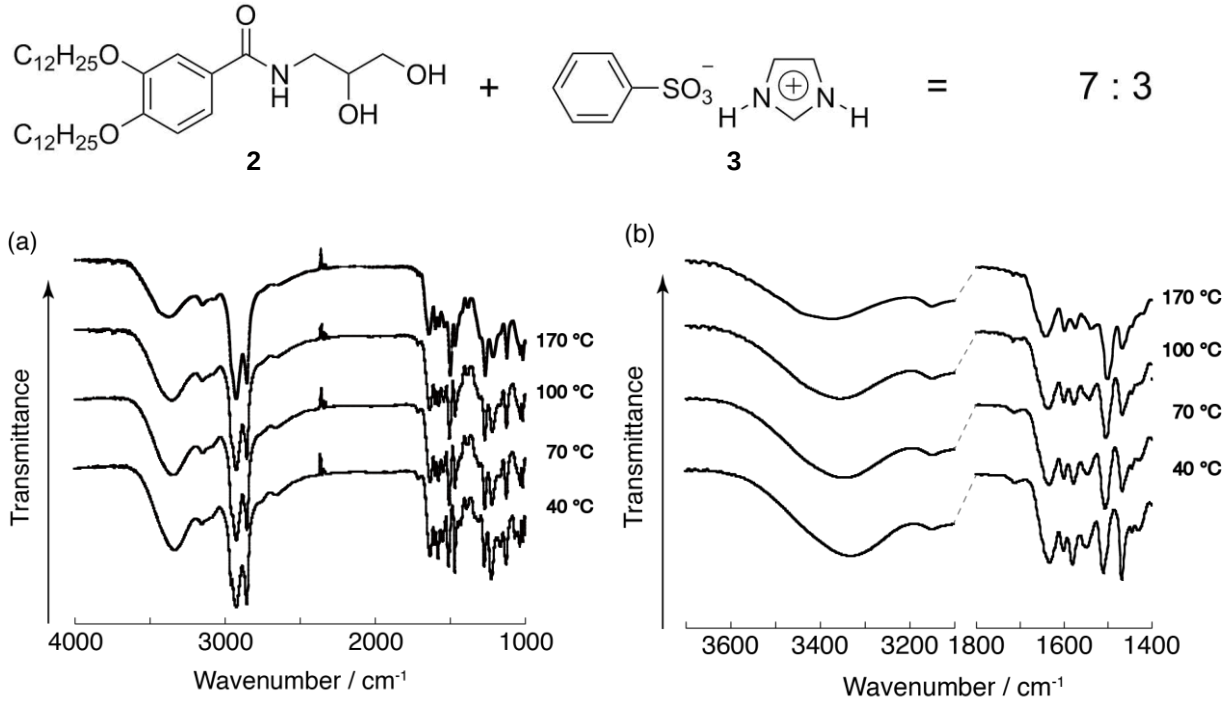

Figure S15. (a) Temperature dependent FT-IR spectra of the mixture **2**/**3**(30) and (b) its enlarged view.

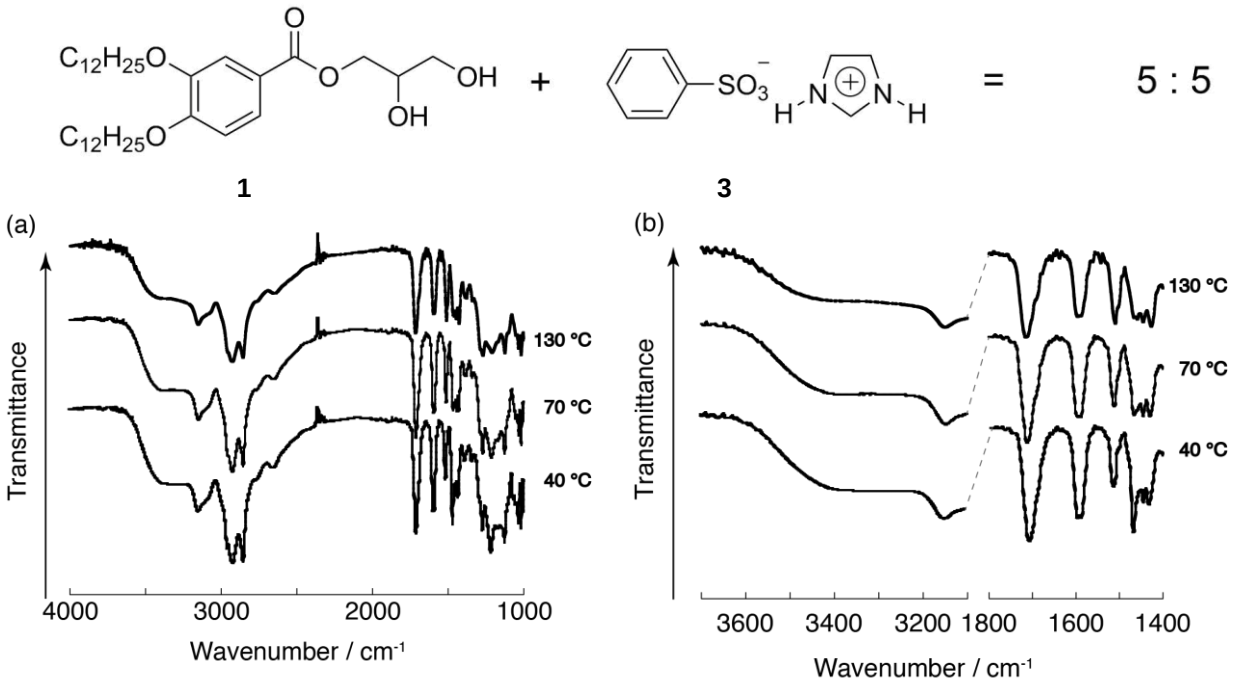

Figure S16. (a) Temperature dependent FT-IR spectra of the mixture **1**/**3**(50) and (b) its enlarged view.

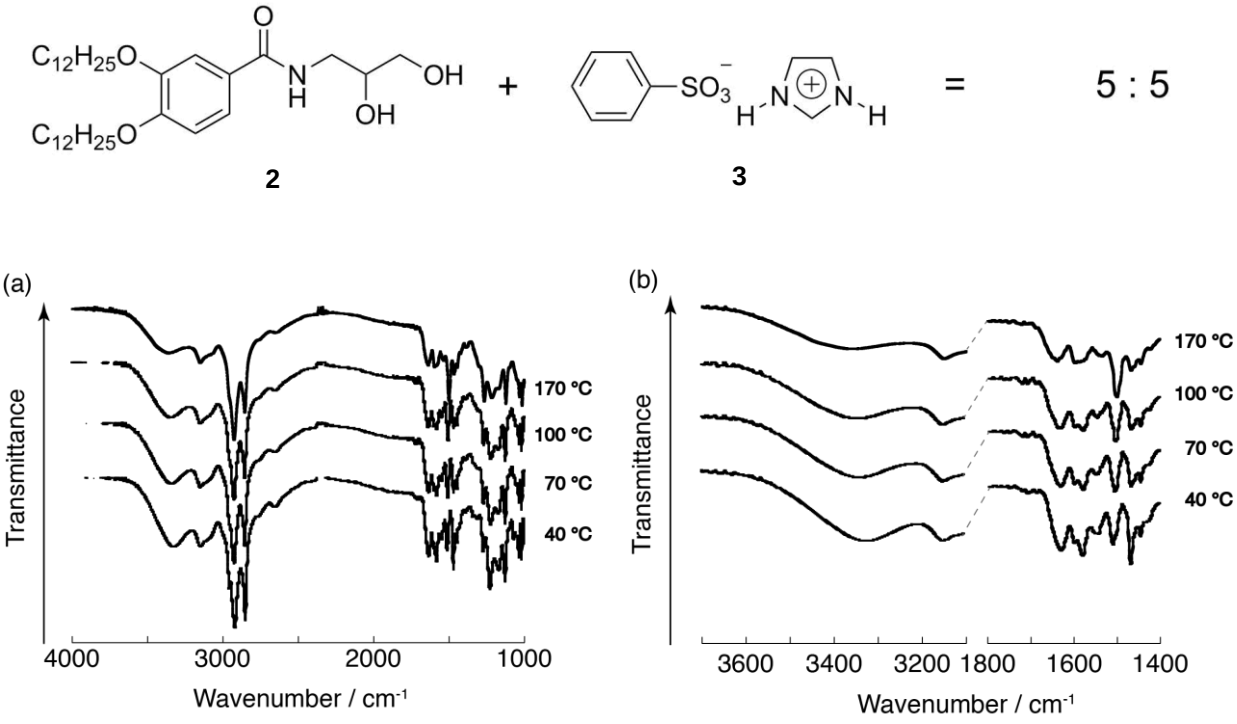

Figure S17. (a) Temperature dependent FT-IR spectra of the mixture **2**/**3**(50) and (b) its enlarged view.

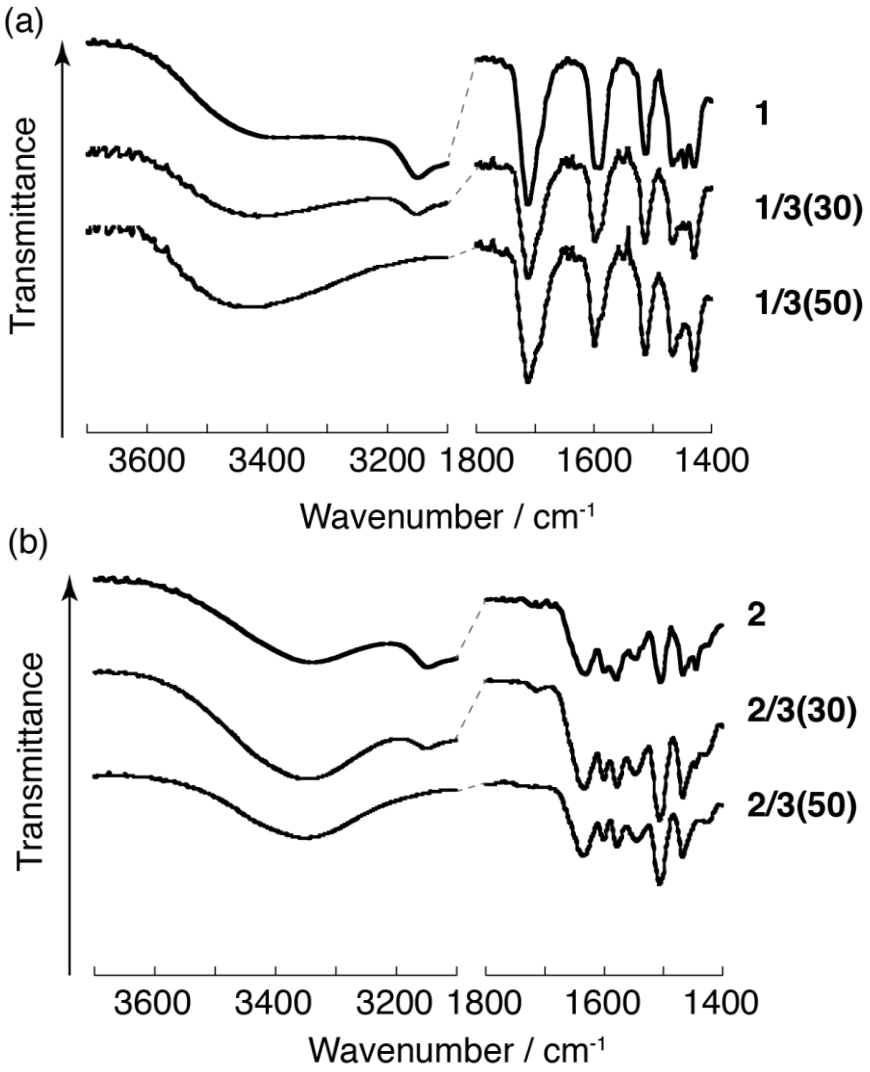

Figure S18. FT-IR spectra of (a) the mixtures of compound **1** and protic salt **3** and (b) the mixtures of compound **2** and protic salt **3** at 70 °C.

7. POM images of the uniaxially oriented 2/3(20) in the Col_h phase

A uniaxially parallel orientation of the columns of the mixture **2**/**3**(20) has been achieved between the comb-shaped gold electrodes on a glass substrate by the application of mechanical shear force to the sample at 120 °C.

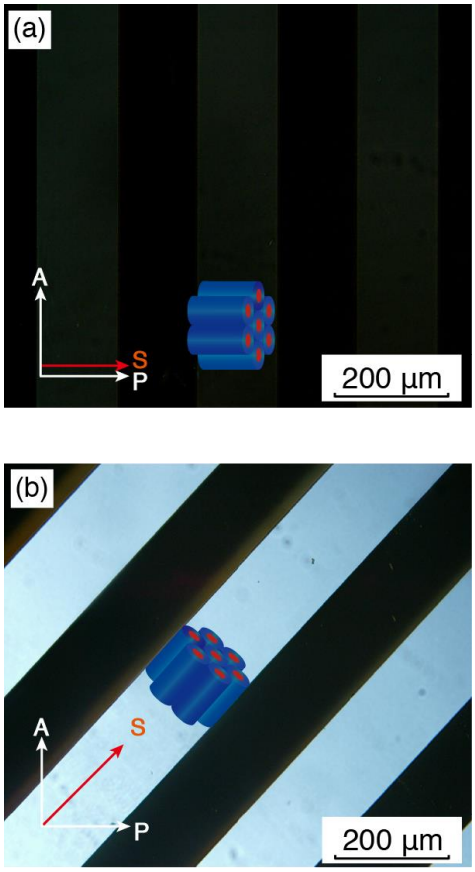

Figure S19. POM images of the uniaxially oriented mixture **2**/**3**(20) under a crossed Nicols condition. (a) The shearing direction is parallel to the polarizer axis. (b)The sample of (a) is rotated by 45 °. Arrows indicate the directions of the shear force (S), analyzer (A) and polarizer (P) axes.

8. Vogel-Tamman-Fulcher plots of the ionic conductivities for mixtures 1/3(x) and 2/3(x)

The temperature dependence of the ionic conductivities for the mixtures **1**/**3**(x) and **2**/**3**(x), where x denotes the mole% of **3**, are fitted by the Vogel-Tamman-Fulcher (VTF) equation:

$$\sigma = \frac{A}{\sqrt{T}} exp\left(\frac{-B}{T - T_0}\right)$$

where σ and T are the ionic conductivity and the absolute temperature. A, B and T_0 are fitting parameters. The parameter A (S m^{-1} $K^{1/2}$) is related to the carrier ion number. The parameter B (K) is related to the activation energy. The product of B (K) and the molar gas constant (8.31 J K^{-1} mol^{-1}) has the dimension of activation energy (J mol^{-1}). T_0 (K) is the ideal glass transition temperature at which the configurational entropy vanishes.

The temperature dependencies of ionic conductivities for the mixtures **1**/**3**(x) and **2**/**3**(x) are well fitted by the VTF equation. The VTF fitting parameters are summarized in Table S1. For example, the VTF fitting of the ionic conductivities for the mixture **2**/**3**(20) in the Col_h phase is shown in Figure S20. The VTF plots of the ionic conductivities for the mixtures **1**/**3**(x) and **2**/**3**(x) shown in Figure S21 are depicted as straight lines.

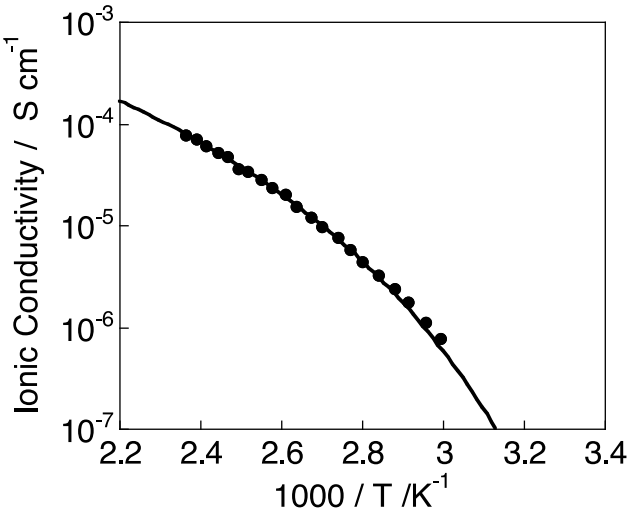

Figure S20. Arrhenius plots for the ionic conductivity of the mixture **2**/**3**(20). The solid line is the fitting result of the value of ionic conductivity on the VTF equation.

Table S1. VTF fitting parameters of the ionic conductivities for mixtures **1**/**3**(x) and **2**/**3**(x).

	A (S m^{-1} K$^{1/2}$)	B (K)	T_0 (K)	R^2
1/**3**(20)	0.032	625.9	238.8	0.9983
1/**3**(30)	0.121	751.3	229.7	0.9991
1/**3**(50)	13.10	2161.1	124.82	0.9972
2/**3**(20)	0.049	877.71	242.34	0.9984
2/**3**(30)	0.173	847.73	239.43	0.9996
2/**3**(50)	14.35	2480.1	128.02	0.9986

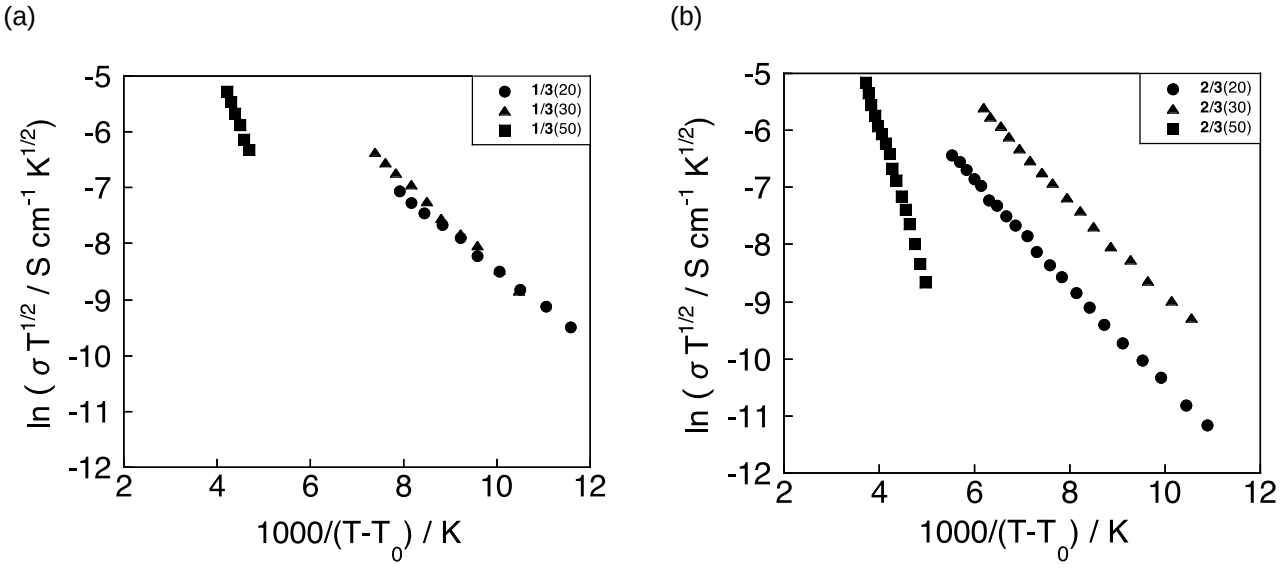

Figure S21. VTF plots of the ionic conductivities for (a) the mixture **1**/**3**(x) and (b) the mixture **2**/**3**(x) in the liquid-crystalline phases. The mixtures **1**/**3**(20), **1**/**3**(30), **2**/**3**(20), and **2**/**3**(30) form the Col_h phases. The mixtures **1**/**3**(50) and **2**/**3**(50) exhibit the S_A phases.

9. DSC thermograms of 1, 2 and their mixtures with 3

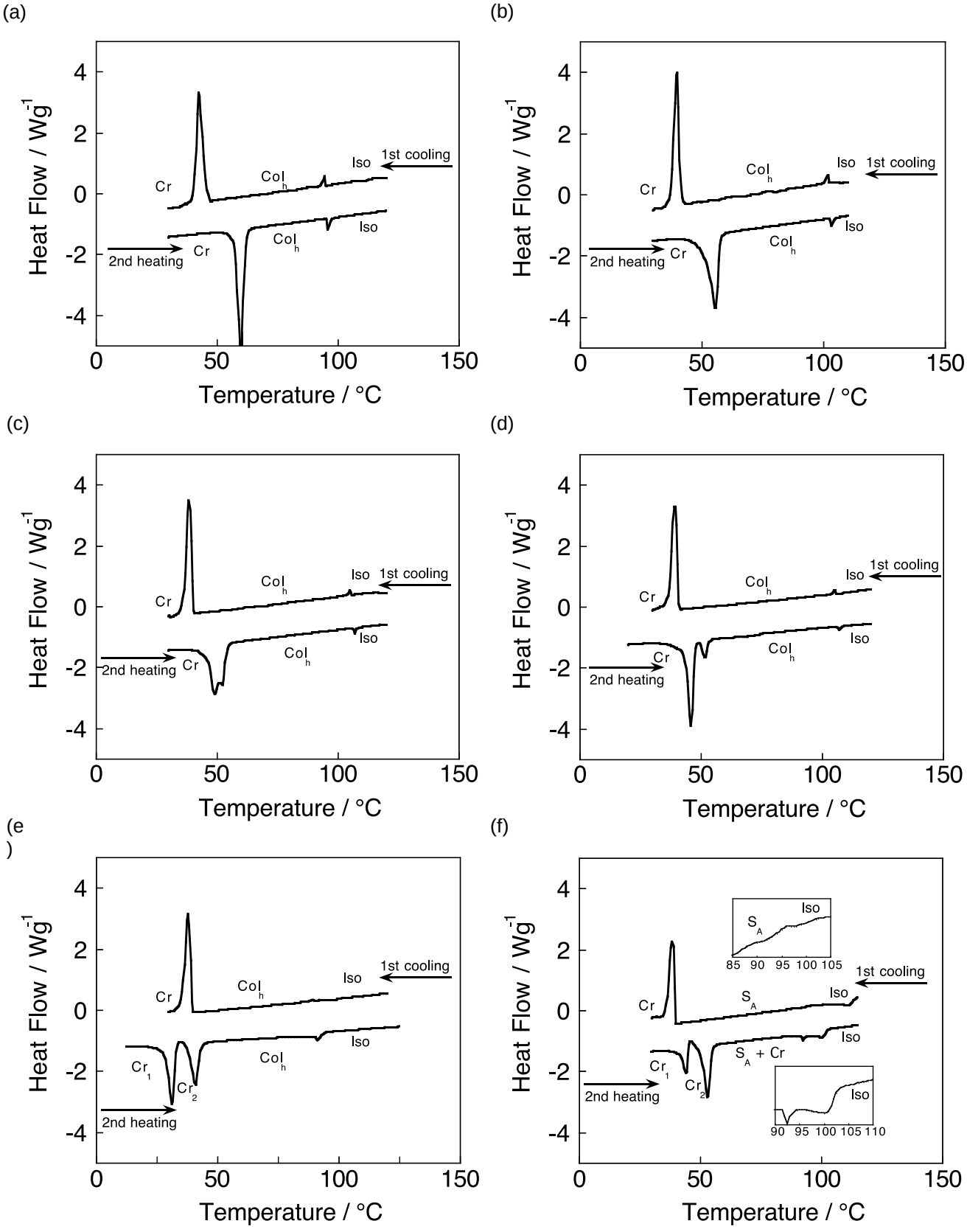

Figure S22. DSC thermograms of (a) compound **1**, (b) mixture **1**/**3**(10), (c) mixture **1**/**3**(20), (d) mixture **1**/**3**(30), (e) mixture **1**/**3**(40), and (f) mixture **1**/**3**(50) at the scanning rate of 10 K/min.

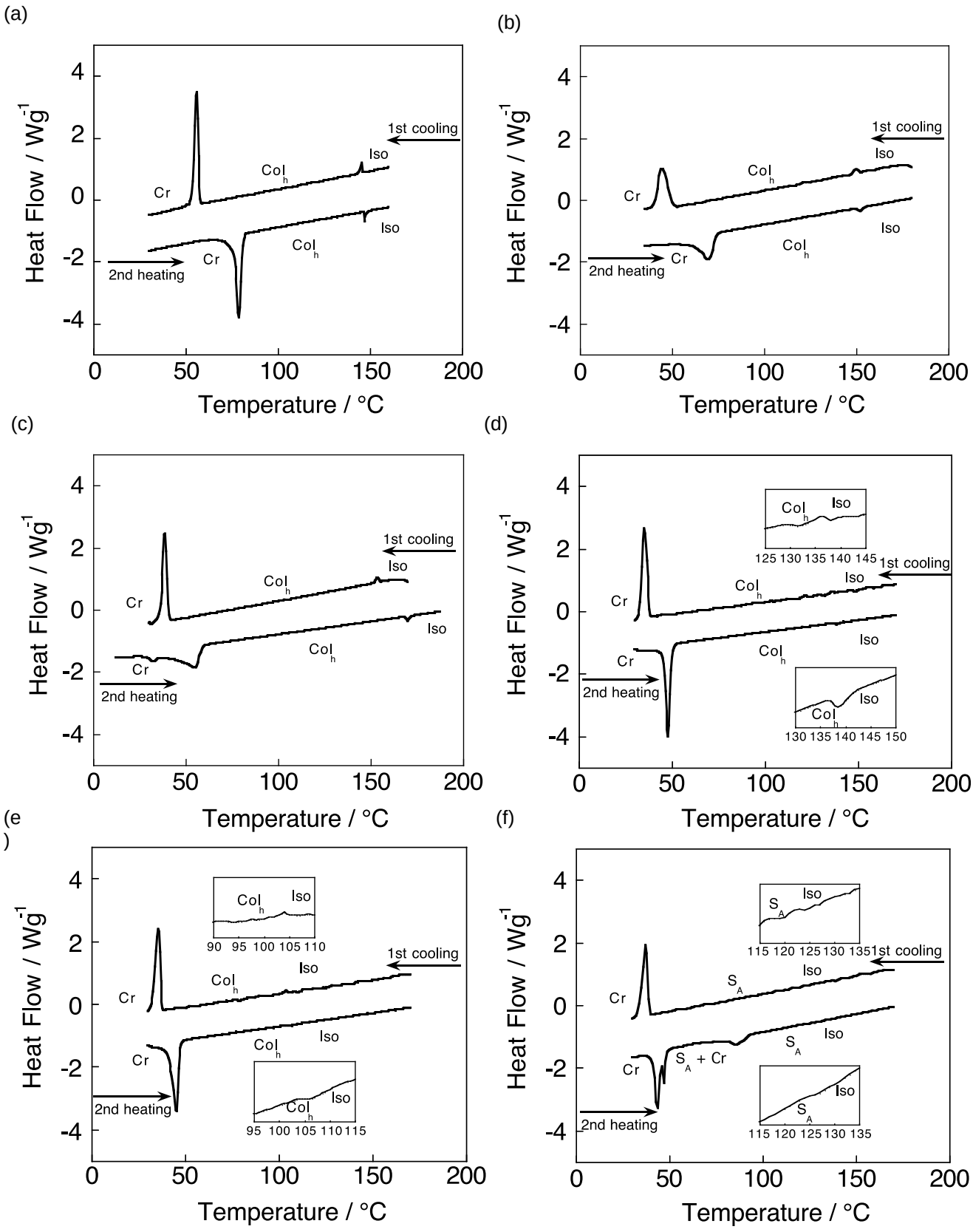

Figure S23. DSC thermograms of (a) compound **2**, (b) mixture **2**/**3**(10), (c) mixture **2**/**3**(20), (d) mixture **2**/**3**(30), (e) mixture **2**/**3**(40), and (f) mixture **2**/**3**(50) at the scanning rate of 10 K/min.

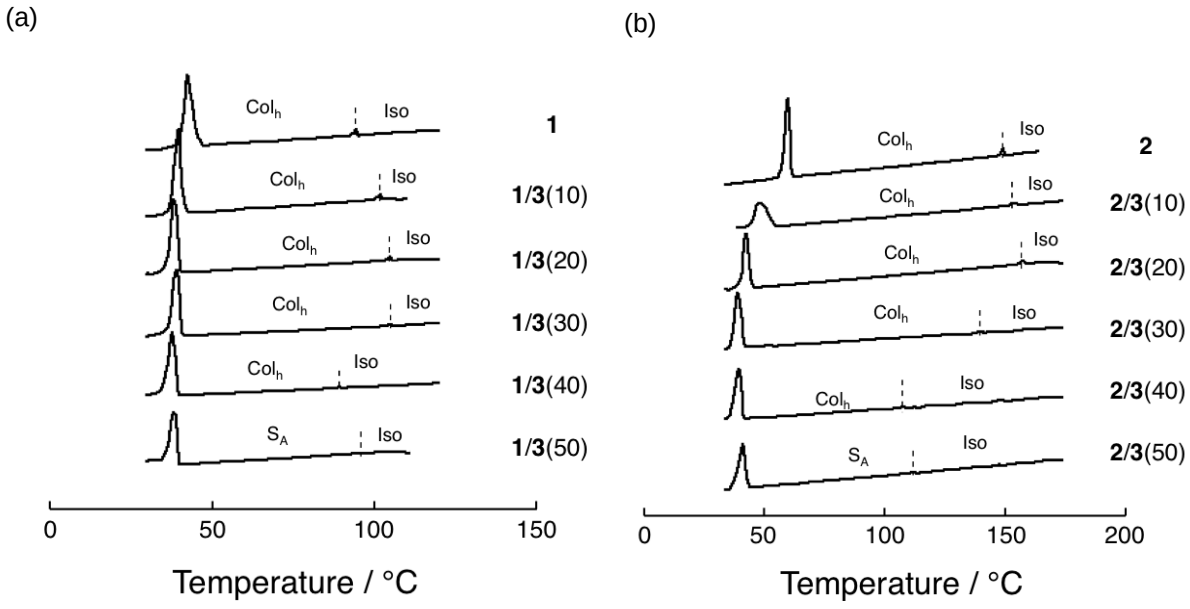

Figure S24. DSC thermograms of (a) the mixtures **1**/**3**(x) and (b) the mixtures **2**/**3**(x) on cooling at the scanning rate of 10 K/min.

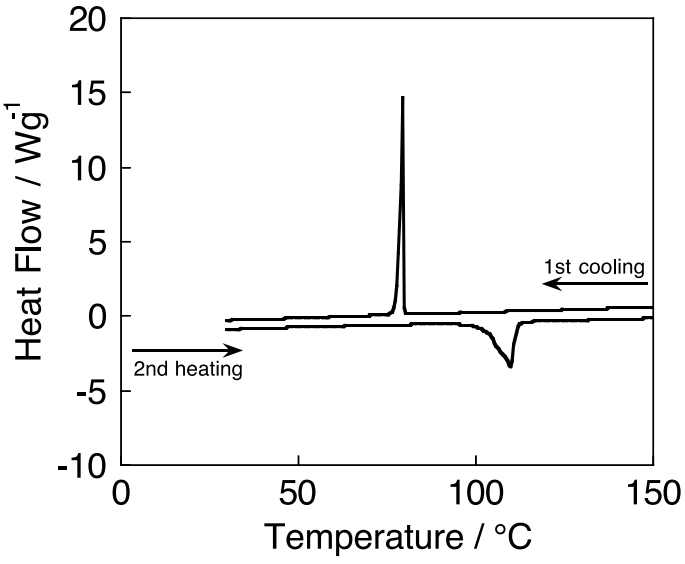

Figure S25. DSC thermograms of protic salt **3** at the scanning rate of 10 K/min.

10. Wide-angle XRD diffraction patterns of the mixtures

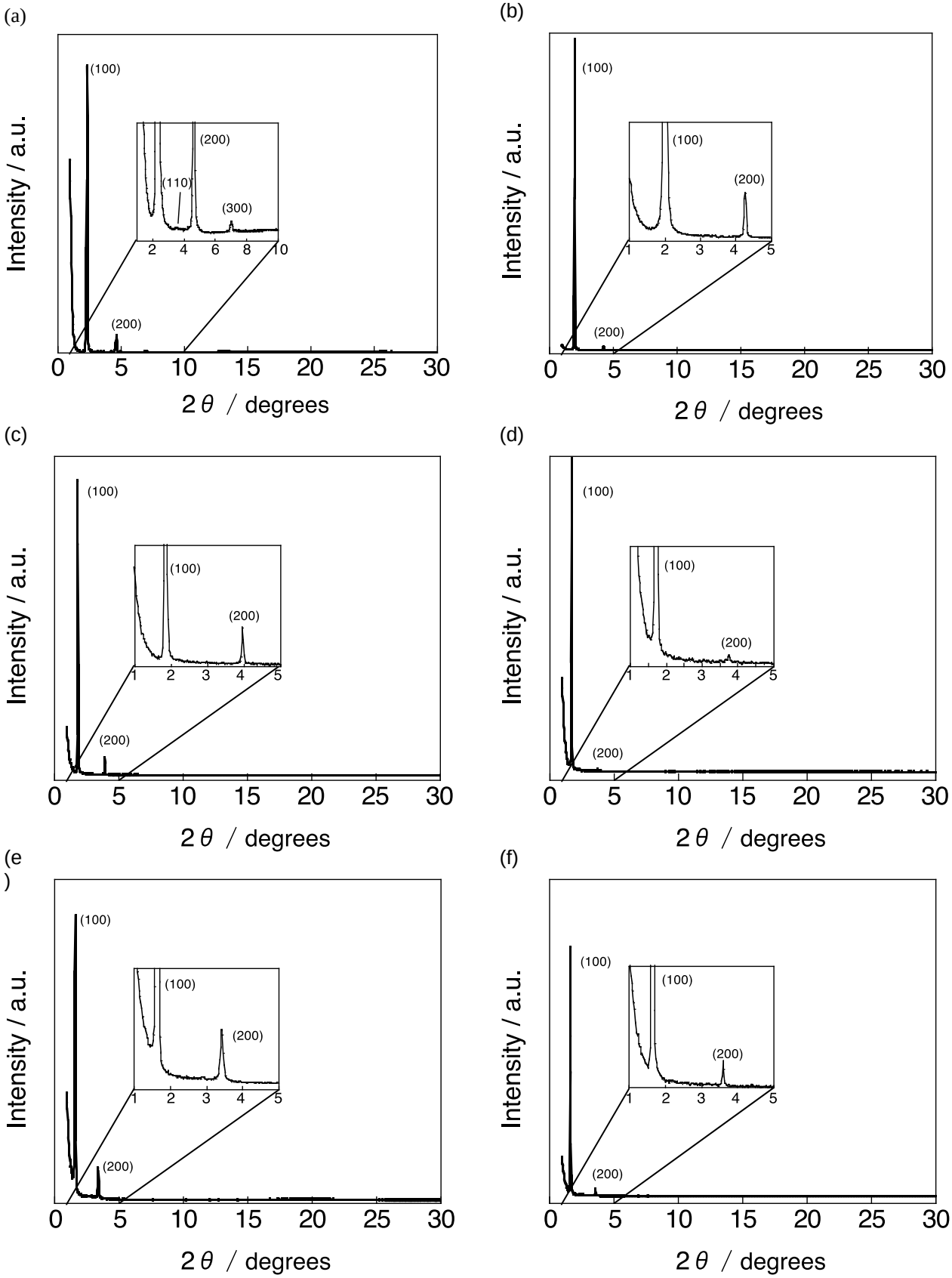

Figure S26. Wide-angle XRD patterns of (a) compound **1**, (b) mixture **1**/**3**(10), (c) mixture **1**/**3**(20), (d) mixture **1**/**3**(30), (e) mixture **1**/**3**(40), and (f) mixture **1**/**3**(50) at 70 °C.

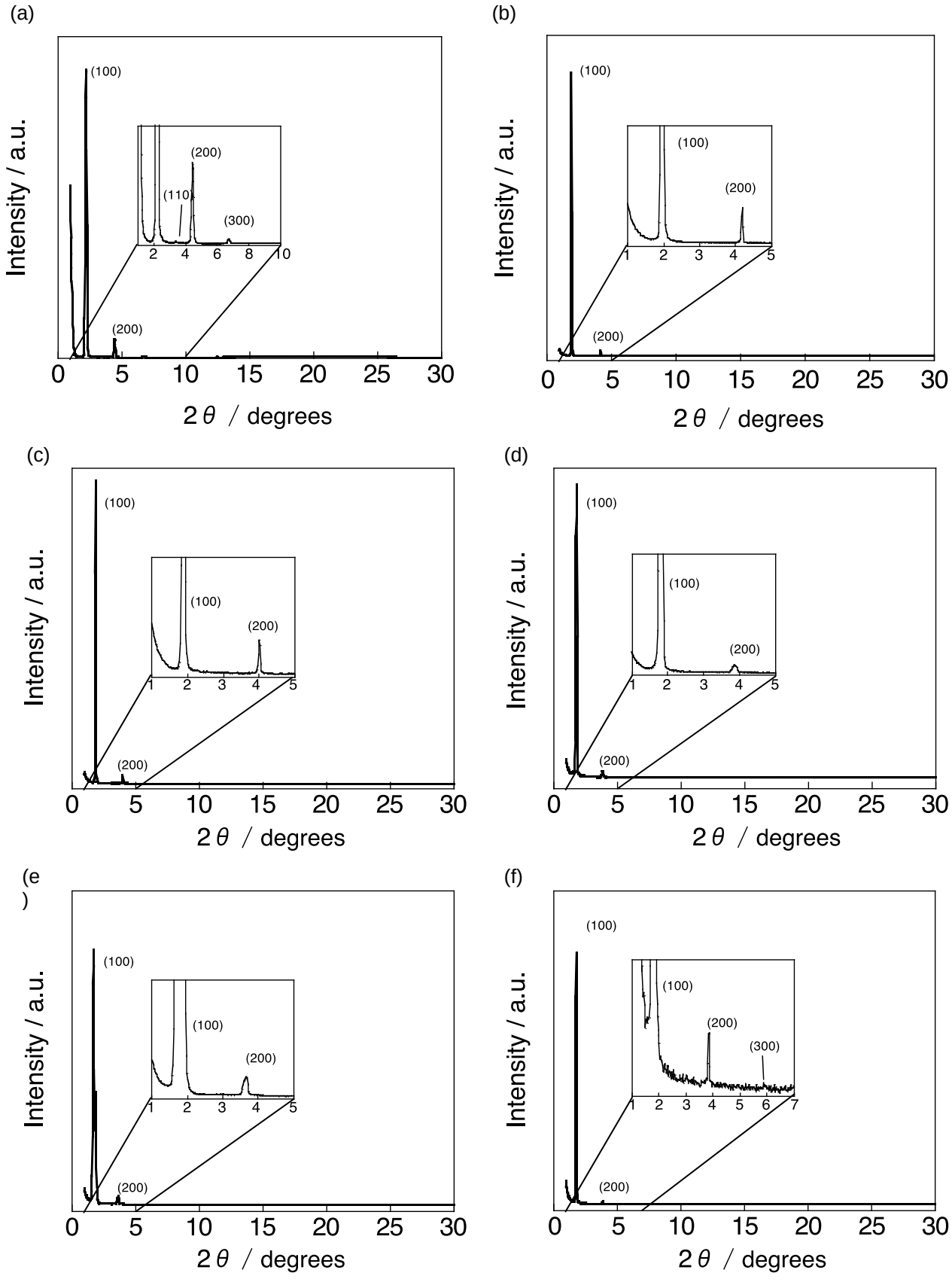

Figure S27. Wide-angle XRD patterns of (a) compound **2**, (b) mixture **2**/**3**(10), (c) mixture **2**/**3**(20), (d) mixture **2**/**3**(30), (e) mixture **2**/**3**(40), and (f) mixture **2**/**3**(50) at 70 °C.

Table S2. The values of *d*-spacing for the mixtures **1**/**3**(x) at 70 °C.

	(100) [Å]	(200) [Å]
1	39.41	19.71
1/**3**(10)	45.04	21.02
1/**3**(20)	46.95	21.96
1/**3**(30)	47.97	22.87
1/**3**(40)	50.73	23.99
1/**3**(50)	49.04	22.75

Table S3. The values of *d*-spacing for the mixtures **2**/**3**(x) at 70 °C.

	(100) [Å]	(200) [Å]
2	37.72	18.87
2/**3**(10)	44.14	20.63
2/**3**(20)	47.97	22.29
2/**3**(30)	50.73	23.36
2/**3**(40)	55.17	25.66
2/**3**(50)	49.04	22.87

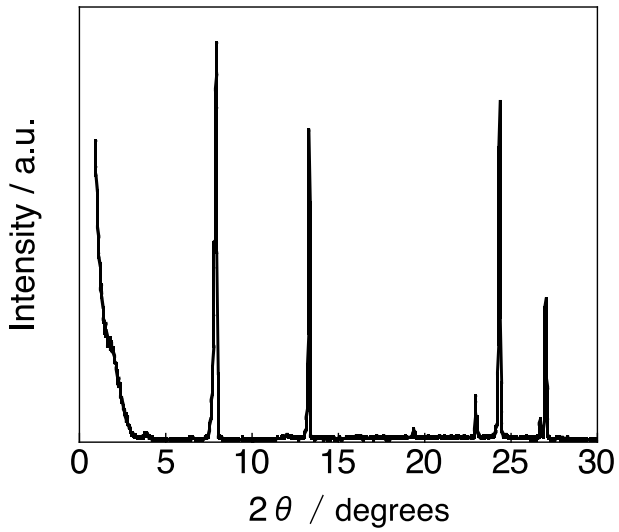

Figure S28. Wide-angle XRD pattern of protic salt **3** at 25 °C.